Localized surface plasmon resonance in arrays of nano-gold cylinders: inverse problem and propagation of uncertainties

Dominique Barchiesi, [1,*] **Sameh Kessentini,** [1] **Nicolas Guillot,** [2] **Marc Lamy de la Chapelle,**[2] **and Thomas Grosges**[1]

[1] *Project Group for Automatic Mesh Generation and Advanced Methods, Gamma3 project (UTT-INRIA), University of Technology of Troyes – 12 Rue Marie Curie – CS 42060, 10004 Troyes Cedex, France*

[2] *CSPBAT Laboratory - UMR CNRS 7244 - University of Paris 13 74 Rue Marcel CACHIN - FR-93017 Bobigny Cedex, France*

[*] *dominique.barchiesi@utt.fr*

Abstract: The plasmonic nanostructures are widely used to design sensors with improved capabilities. The position of the localized surface plasmon resonance (LSPR) is part of their characteristics and deserves to be specifically studied, according to its importance in sensor tuning, especially for spectroscopic applications. In the visible and near infra-red domain, the LSPR of an array of nano-gold-cylinders is considered as a function of the diameter, height of cylinders and the thickness of chromium adhesion layer and roughness. A numerical experience plan is used to calculate heuristic laws governing the inverse problem and the propagation of uncertainties. Simple linear formulae are deduced from fitting of discrete dipole approximation (DDA) calculations of spectra and a good agreement with various experimental results is found. The size of cylinders can be deduced from a target position of the LSPR and conversely, the approximate position of the LSPR can be simply deduced from the height and diameter of cylinders. The sensitivity coefficients and the propagation of uncertainties on these parameters are evaluated from the fitting of 15500 computations of the DDA model. The case of a grating of nanodisks and of homothetic cylinders is presented and expected trends in the improvement of the fabrication process are proposed.

OCIS codes: (250.5403) Plasmonics; (100.3190) Inverse problems; (000.4430) Numerical approximation and analysis; (350.4600) Optical engineering; (130.6010) Sensors.

References and links

1. E. C. Le Ru and P. G. Etchegoin, *Principles of sSurface-Enhanced Raman Spectroscopy and Related Plasmonic Effects* (Elsevier, Amsterdam, 2009).
2. M. Vidotti, R. F. Carvalhal, R. K. Mendes, D. C. M. Ferreira, and L. T. Kubota, "Biosensors based on gold nanostructures," J. Braz. Chem. Soc. **22**, 3–20 (2011).
3. S. A. Maier, *Plasmonics. Fundamentals and Applications* (Springer, New York, USA, 2007).
4. J. Grand, M. Lamy de la Chapelle, J.-L. Bijeon, P.-M. Adam, A. Vial, and P. Royer, "Role of localized surface plasmons in surface-enhanced Raman scattering of shape-controlled metallic particles in regular arrays," Phys. Rev. B **72**, 033407 (2005).

#179498 - $15.00 USD Received 7 Nov 2012; revised 21 Dec 2012; accepted 9 Jan 2013; published 23 Jan 2013

5. N. Félidj, J. Aubard, G. Lévi, J. R. Krenn, M. Salerno, G. Schider, B. Lamprecht, A. Leitner, and F. R. Aussenegg, "Controlling the optical response of regular arrays of gold particles for surface-enhanced Raman scattering," Phys. Rev. B **65**, 075419–075427 (2002).
6. N. Félidj, J. Aubard, G. Lévi, J. R. Krenn, A. Hohenau, G. Schider, A. Leitner, and F. R. Aussenegg, "Optimized surface-enhanced Raman scattering on gold nanoparticles arrays," Appl. Phys. Lett. **82**, 3095–3097 (2003).
7. A.-S. Grimault, A. Vial, and M. Lamy de la Chapelle, "Modeling of regular gold nanostructures arrays for SERS applications using a 3D FDTD method," Appl. Phys. B-Lasers Opt. **84**, 111–115 (2006).
8. N. Guillot, H. Shen, B. Frémaux, O. Péron, E. Rinnert, T. Toury, and M. Lamy de la Chapelle, "Surface enhanced Raman scattering optimization of gold nanocylinder arrays: influence of the localized surface plasmon resonance and excitation wavelength," Appl. Phys. Lett. **97**, 023113–023116 (2010).
9. H.-H. Yan, Y.-Y. Xiao, S.-X. Xie, and H.-J. Li, "Tunable plasmon resonance of a touching gold cylinder arrays," J. At. Mol. Sci. **3**, 252–261 (2012).
10. A. Dasgupta and G. V. P. Kumar, "Palladium bridged gold nanocylinder dimer: plasmonic properties and hydrogen sensitivity," Appl. Opt. **51**, 1688–1693 (2012).
11. B. Lamprecht, G. Schider, R. T. Lechner, H. Diltbacher, J. R. Krenn, A. Leitner, and F. R. Aussenegg, "Metal nanoparticles gratings: influence of dipolar interaction on the plasmon resonance," Phys. Rev. Lett. **84**, 4721–4723 (2000).
12. S. Davy, D. Barchiesi, M. Spajer, and D. Courjon, "Spectroscopic study of resonant dielectric structures in near–field," Eur. Phys. J.-Appl. Phys., **5**, 277–281 (1999).
13. D. Barchiesi, "Pseudo modulation transfer function in reflection scanning near-field optical microscopy," Opt. Commun. **154**, 167–172 (1998).
14. J. Grand, *Plasmons de surface de nanoparticules : spectroscopie d'extinction en champs proche et lointain, diffusion Raman exaltée*, Ph.D. thesis (Université de technologie de Troyes, 2004).
15. D. Barchiesi, D. Macías, L. Belmar-Letellier, D. Van Labeke, M. Lamy de la Chapelle, T. Toury, E. Kremer, L. Moreau, and T. Grosges, "Plasmonics: influence of the intermediate (or stick) layer on the efficiency of sensors," Appl. Phys. B-Lasers Opt. **93**, 177–181 (2008).
16. S. Kessentini and D. Barchiesi, "Roughness effect on the efficiency of dimer antenna based biosensor," Advanced Electromagnetics (AEM) **1**, 41–47 (2012).
17. L. Billot, M. Lamy de la Chapelle, A. S. Grimault, A. Vial, D. Barchiesi, J.-L. Bijeon, , P.-M. Adam, and P. Royer, "Surface enhanced Raman scattering on gold nanowire arrays: evidence of strong multipolar surface plasmon resonance enhancement," Chem. Phys. Lett. **422**, 303–307 (2006).
18. M. Pelton, J. Aizpurua, and G. W. Bryant, "Metal-nanoparticles plasmonics," Laser & Photon. Rev. **2**, 136–159 (2008).
19. D. Sharma, R. Sharma, S. Dua, and V. N. Ojha, "Pitch measurements of 1D/2D gratings using optical profiler and comparison with SEM /AFM," in *AdMet 2012*, (Metrology Society of India, ARAI, Pune, India, 2012), NM 003, 1–4.
20. G. Laurent, N. Félidj, J. Aubard, G. Lévi, J. R. Krenn, A. Hohenau, G. Schider, A. Leitner, and F. R. Aussenegg, "Evidence of multipolar excitations in surface enhanced Raman scattering," Phys. Rev. B **65**, 045430 (2005).
21. D. Barchiesi, E. Kremer, V. Mai, and T. Grosges, "A Poincaré's approach for plasmonics: the plasmon localization," J. Microscopy **229**, 525–532 (2008).
22. C. F. Bohren and D. R. Huffman, *Absorption and Scattering of Light by Small Particles* (John Wiley & Sons, Inc., New York, 1998).
23. A. A. Yanik, M. Huang, A. Artar, T.-Y. Chang, and H. Altug, "On-chip nanoplasmonic biosensors with actively controlled nanofluidic surface delivery," in *Plasmonics: metallic nanostructures and their optical properties VIII*, M. I. Stockman, ed. (SPIE, San Diego, California, USA, 2010), vol. 7757, 775735.
24. X. Huang, S. Neretina, and M. A. El-Sayed, "Gold nanorods: from synthesis and properties to biological and biomedical applications," J. Adv. Mater. **21**, 4880–4910 (2009).
25. Y. B. Zheng, B. K. Juluri, X. Mao, T. R. Walker, and T. J. Huang, "Systematic investigation of localized surface plasmon resonance of long-range ordered Au nanodisk arrays," J. Appl. Phys **103**, 014308 (2008).
26. H. Shen, N. Guillot, J. Rouxel, M. Lamy de la Chapelle, and T. Toury, "Optimized plasmonic nanostructures for improved sensing activities," Opt. Express **20**, 21278–21290 (2012).
27. A. Vial and T. Laroche, "Description of dispersion properties of metals by means of the critical points model and application to the study of resonant structures using the FDTD method," J. Phys. D. **40**, 7152–7158 (2007).
28. D. Barchiesi, N. Lidgi-Guigui, and M. Lamy de la Chapelle, "Functionalization layer influence on the sensitivity of surface plasmon resonance (SPR) biosensor," Opt. Commun. **285**, 1619–1623 (2012).
29. D. Barchiesi, *New perspectives in biosensors technology and applications* (INTECH Open Access, Rijeka, Croatia, 2011), chap. 5, pp. 105–126.
30. H. Aouani, J. Wenger, D. Gérard, H. Rigneault, E. Devaux, T. W. Ebbesen, F. Mahdavi, T. Xu, and S. Blair, "Crucial role of the adhesion layer on the plasmonic fluorescence enhancement," ACS Nano **3**, 2043–2048 (2009).
31. F. D. Hastings, J. B. Schneider, and S. L. Broschat, "A Monte-Carlo FDTD technique for rough surface scattering," IEEE Transactions on antennas and propagation **43**, 1183–1191 (1995).
32. K. M. Byun, S. J. Yoon, D. Kim, and S. J. Kim, "Sensitivity analysis of a nanowire-based surface plasmon

#179498 - $15.00 USD Received 7 Nov 2012; revised 21 Dec 2012; accepted 9 Jan 2013; published 23 Jan 2013

resonance biosensor in the presence of surface roughness," J. Opt. Soc. Am. A **24**, 522–529 (2007).
33. V. Poroshin, Y. Borovin, and D. Bogomolov, "Transfer of the surface roughness geometry into the universal FEM software ANSYS," Advanced Engineering **3**, 1846–5900 (2009).
34. A. Kato, S. Burger, and F. Scholze, "Analytical modeling and three-dimensional finite element simulation in line edge roughness in scatterometry," Appl. Opt. **51**, 6457–6464 (2012).
35. A. Trügler, J.-C. Tinguely, J. R. Krenn, A. Hohenau, and U. Hohenester, "Influence of surface roughness on the optical properties of plasmonic nanoparticles," Phys. Rev. B **83**, 081412 (2011).
36. B. T. Draine and P. J. Flatau, "Discrete-dipole approximation for scattering calculations," J. Opt. Soc. Am. A **11**, 1491–1499 (1994).
37. N. Félidj, J. Aubard, and G. Lévi, "Discrete dipole approximation for ultraviolet-visible extinction spectra simulation of silver and gold colloids," J. Chem. Phys **111**, 1195–1208 (1999).
38. K. L. Kelly, E. Coronado, L. L. Zhao, and G. C. Schatz, "The optical properties of metal nanoparticles: the influence of size, shape, and dielectric environment," J. Phys. Chem. B **107**, 668–677 (2003).
39. K. S. Lee and M. A. El-Sayed, "Dependence of the enhanced optical scattering efficiency relative to that of absorption of gold metal nanorods on aspect ratio, size, end-cap shape, and medium refractive," J. Phys. Chem. B **109**, 20331–20338 (2005).
40. P. K. Jain, K. S. Lee, I. H. El-Sayed, and M. A. El-Sayed, "Calculated absorption and scattering properties of gold nanoparticles of different size, shape, and composition: applications in biological imaging and biomedicine," J. Phys. Chem. **110**, 7238–7248 (2006).
41. B. T. Draine and P. J. Flatau, "Discrete-dipole approximation for periodic targets: theory and tests," J. Opt. Soc. Am. A **25**, 2693–2703 (2008).
42. S. Kessentini and D. Barchiesi, "Quantitative comparison of optimized nanorods, nanoshells and hollow nanospheres for photothermal therapy," Biomed. Opt. Express **3**, 590–604 (2012).
43. H. Devoe, "Optical properties of molecular aggregates. I. Classical model of electronic absorption and refraction," J. Chem. Phys. **41**, 393–400 (1964).
44. H. Devoe, "Optical properties of molecular aggregates. II. Classical theory of the refraction, absorption, and optical activity of solutions and crystals," J. Chem. Phys. **43**, 3199–3208 (1965).
45. E. Purcell and C. R. Pennypacker, "Scattering and absorption of light by nonspherical dielectric grains," Astrophys. J. **186**, 705–714 (1973).
46. V. A. Markel, "Scattering of light from two interacting spherical particles," J. Mod. Opt. **39**, 853–861 (1992).
47. P. C. Chaumet, A. Rahmani, and G. W. Bryant, "Generalization of the coupled dipole method to periodic structures," Phys. Rev. B **67**, 165404(1–5) (2003).
48. E. Zubko, D. Petrov, Y. Grynko, Y. Shkuratov, H. Okamotot, K. Muinonen, T. Nousiainen, H. Kimura, T. Yamamoto, and G. Videen, "Validity criteria of the discrete dipole approximation," Appl. Opt. **49**, 1267–1279 (2010).
49. C. Ungureanu, R. G. Rayavarapu, S. Manohar, and T. G. Van Leeuwen, "Discrete dipole approximation simulations of gold nanorod optical properties: choice of input parameters and comparison with experiment," J. Appl. Phys. **105**, 102032–102039 (2009).
50. W.-H. Yang, G. C. Schatz, and R. P. Van Duyne, "Discrete dipole approximation for calculating extinction and Raman intensities for small particles with arbitrary shapes," J. Chem. Phys. **193**, 869–875 (1995).
51. H. Parviainen and K. Lumme, "Scattering from rough thin films: discrete-dipole-approximation simulations," J. Opt. Soc. Am. A **25**, 90–97 (2008).
52. B. T. Draine and P. J. Flatau, "User guide to the discrete dipole approximation code DDSCAT 7.1," http://arXiv.org/abs/1002.1505v1 (2010).
53. A. J. Haija, W. L. Freeman, and T. Roarty, "Effective characteristic matrix of ultrathin multilayer structures," Opt. Appl. **36**, 39–50 (2006).
54. A. J. Abu El-Haija, "Effective medium approximation for the effective optical constants of a bilayer and a multilayer structure based on the characteristic matrix technique," J . Appl. Phys. **93**, 2590–2594 (2003).
55. D. Barchiesi, "Numerical retrieval of thin aluminium layer properties from SPR experimental data," Opt. Express **20**, 9064–9078 (2012).
56. P. Johnson and R. W. Christy, "Optical constants of the noble metals," Phys. Rev. B **6**, 4370 (1972).
57. E. D. Palik, *Handbook of Optical Constants* (Academic Press Inc., San Diego USA, 1985).
58. S. Ekgasit, C. Thammacharoen, F. Yu, and W. Knoll, "Influence of the metal film thickness on the sensitivity of surface plasmon resonance biosensors," Appl. Spectrosc. **59**, 661–667 (2005).
59. H. Neff, W. Zong, A. Lima, M. Borre, and G. Holzhüter, "Optical properties and instrumental performance of thin gold films near the surface plasmon resonance," Thin Solid Films **496**, 688–697 (2006).
60. B. A. Sexton, B. N. Feltis, and T. J. Davis, "Effect of surface roughness on the extinction-based localized surface plasmon resonance biosensor," Sens. Actuator A-Phys. **141**, 471475 (2008).
61. Working Group 1, *Evaluation of measurement data - Guide to the expression of uncertainty in measurement*, (Joint Committee for Guides in Metrology, Paris, 1st ed., 2008, Corrected version 2010).
62. D. Macías, A. Vial, and D. Barchiesi, "Application of evolution strategies for the solution of an inverse problem in Near-Field Optics," J. Opt. Soc. Am. A **21**, 1465–1471 (2004).

#179498 - $15.00 USD Received 7 Nov 2012; revised 21 Dec 2012; accepted 9 Jan 2013; published 23 Jan 2013

63. T. Grosges, D. Barchiesi, T. Toury, and G. Gréhan, "Design of nanostructures for imaging and biomedical applications by plasmonic optimization," Opt. Lett. **33**, 2812–2814 (2008).
64. D. Macías, A. Vial, and D. Barchiesi, "Evolution strategies approach for the solution of an inverse problem in near-field optics," in *Lecture notes in computer science (6e European Workshop on Evolutionary Computation in Image Analysis and Signal Processing)* , vol. 3005 / 2004, G. Raidl, S. Cagnoni, J. Branke, R. Corne, D. W. Drechsler, Y. Jin, C. Johnson, P. Machado, E. Marchiori, F. Rothlauf, G. Smith, and G. Squillero, eds. (Springer-Verlag Heidelberg, Germany, 2004), 329 –338.
65. D. Barchiesi and T. Grosges, "Measurement of the decay lengths of the near field signal in tapping mode," Curr. Appl. Phys. **9**, 1227–1231 (2009).
66. D. Barchiesi, O. Bergossi, M. Spajer, and C. Pieralli, "Image resolution in reflection scanning near-field optical microscopy (R-SNOM) using shear-force (ShF) feedback: characterization using spline and Fourier spectrum," Appl. Opt. **36**, 2171–2177 (1997).
67. T. Grosges, D. Barchiesi, S. Kessentini, G. Gréhan, and M. Lamy de la Chapelle, "Nanoshells for photothermal therapy: a Monte-Carlo based numerical study of their design tolerance," Biomed. Opt. Express **2**, 1584–1596 (2011).
68. K. J. Prashant, X. Huang, I. H. El-Sayed, and M. A. El-Sayed, "Calculated absorption and scattering properties of gold nanoparticles of different size, shape and composition: Application in biological imaging and biomedicine," Accounts Chem. Res. **41**, 1578–1586 (2008).

1. Introduction

Arrays of metallic nanostructures have been extensively studied as they are known to be efficient and tunable [1, 2]. The underlying physical phenomenon is the localized surface plasmon resonance (LSPR). According to Maier, "Localized surface plasmons are non-propagating excitations of the conduction electrons of metallic nanostructures coupled to the electromagnetic field... The curved surface of the particles exerts an effective restoring force of the driven electrons, so that a resonance can arise, leading to field amplification both inside and in the near-field zone outside the particle." [3].

The spectral position of the LSPR $\lambda_0(LSPR)$ can therefore be tuned by modifying the shape and size of the nanoparticles and be adapted to the specific excitation of molecules deposited on the nanoparticle surface. Obvious applications of plasmonic devices are biosensors. A periodic arrangement of nanoparticles is used to increase the sensitivity of the biosensor. The prolate and oblate exhibit LSPRs which are related to their asymmetry, leading to a distribution of energy in different LSPR modes [4]. Coupling between transverse and longitudinal LSPR occurs. To prevent this effect which could decrease the efficiency of the biosensor, arrays of gold cylindric nanoparticles have been extensively studied [4–10]. In that papers, the tuning of the LSPR has been proved by varying the diameter of nanocylinders or seldom their height. In the investigated domain of wavelengths, some linear behaviors can be observed when the characteristic sizes of cylindrical nanoparticles were varied.

Based on those results, we propose a basic approach of the inverse problem to deduce analytical laws for the LSPR and then to deduce propagation of uncertainties and tolerance study for the fabrication of nano-gold cylinder based biosensors.

The inverse problem usually goes through an initial stage of modeling of the phenomenon, called direct problem which describes how the parameters of the model translate into experimentally observable LSPR shifts. The key parameters of the problem are identified and also the most likely approximation of their behavior for a given list of $\lambda_0(LSPR)$ (Sec. 2). Then, obtained from systematic numerical experiments, the approach will be to deduce the analytical function giving the LSPR position as a function of the key parameters. This resolution can be done analytically, if the relationship between parameters and $\lambda_0(LSPR)$ is an invertible function of the key parameters (Sec. 3). The result helps to obtain an heuristic formula for $\lambda_0(LSPR)$ within the investigated domain of parameters (Sec. 4). The propagation of uncertainties and therefore the tolerance of fabrication of such nano-device are deduced. A final validation of the solution of the inverse problem with some experimental data is finally proposed (Sec. 5).

#179498 - $15.00 USD Received 7 Nov 2012; revised 21 Dec 2012; accepted 9 Jan 2013; published 23 Jan 2013

The typical parameters of the array of nanocylinders are firstly discussed before presenting the model of the interaction between light and array of nanocylinders. Then it is used within a systematic study of the geometric parameters within domains of variation of previously published experimental data.

2. The array of nanocylinders, experimental uncertainties

The Fig. 1 shows a schematic of the array of nanocylinders. All the parameters related to the experiments can be found in [8]. A grating of gold nanocylinders is deposited on a glass substrate. The distance between cylinders P is supposed to be fixed to 200 nm. Let us note that the periodicity of the grating may influence the detected position of the LSPR [5, 11], in particular in the case of an homogeneous-evanescent switch of a diffracted order [12, 13]. Experimental studies have shown that a variation of the period $P+D = 200 \pm 50$ nm, leads to a LSPR shift lower than 20 nm [14, p. 67]. [5] observed a redshift of 14 nm observed when the interparticle distance P was varied from 200 to 300 nm. Therefore the influence of the experimental uncertainty on this parameter is neglected on the contrary of those on the height and on the diameter of nanocylinders. We focus on the systematic study of the position of LSPR as a function of the diameter D and height h of the gold nanocylinders. The thickness e of the chromium adhesion layer and the roughness of surfaces are included in the model [15, 16].

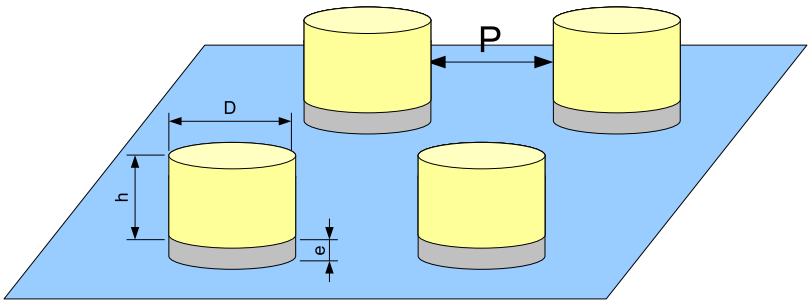

Fig. 1. Biosensor: grating of gold cylinders with diameter D, height h and period $P+D$. The gold nanostructures are deposited on a glass substrate. A layer of Chromium of thickness e is used to improve adhesion of gold on glass.

The nanostructures are deposited on a glass substrate through electron beam lithography (EBL) and lift-off techniques. To achieve EBL, a 30 kV Hitachi S-3500N scanning electron microscope (SEM) equipped with nanometer pattern generation system (NPGS, by J.C. Nabity) are used [17]. The SEM images [4, 5, 8, 14, 18] reveal the experimental sources of uncertainties on the geometrical parameters in the process of fabrication:

- Height (h): the maximum uncertainty is $\delta_h = \pm 2$ nm. This value is due to both the roughness and the process of metal deposition. The SEM images and AFM (Atomic Force Microscopy) scans reveal a RMS (root of mean square) lower than one nanometer [14].
- Thickness (e): the maximum uncertainty is also $\delta_e \pm 2$ nm, but may depend on the thickness of the intermediate layer.
- Diameter (D): the maximum uncertainty is $\delta_D = \pm 20$ nm. This value is relative to both the fabrication and the resolution of the SEM [19] and to a drift of diameter and shape on the whole grating. This last source of uncertainty is evaluated through statistics on the SEM images and is compatible with that found in literature [20].

#179498 - $15.00 USD Received 7 Nov 2012; revised 21 Dec 2012; accepted 9 Jan 2013; published 23 Jan 2013

In the following, the model is used to investigate the propagation of uncertainties on the position of the LSPR. The experimental uncertainties are highly dependent on the process of fabrication of the nanostructures. Among all parameters the roughness of gold nanostructures varies when annealing of sample is used. However, the proposed method remains functional provided the uncertainties are experimentally characterized.

The illumination comes parallel to the cylinder axis and is linearly polarized. The detection of the LSPR is carried out in transmission, in the same direction (in the specular direction) and in far field. Spectroscopic studies are experimentally performed and the maximum of extinction over the incoming wavelengths λ_0 is supposed to reveal the LSPR position [21]. It is commonly admitted that the nanostructures scatters and absorbs a part of the incoming light and that the detected intensity in transmission reveals the extinction of the illumination by the sample [1,22].

3. Model of the interaction of light with nanocylinders array

The fabrication process of nanodevices has been continuously improved and more control and precision were achieved [23,24] but a residual roughness remains on the nanostructures. Indeed, the process of deposition of metal on the substrate is subject to incertitudes on the size of the nanostructures that are generally rough [5, 6, 8, 25, 26]. Usually, roughness is neglected in the models because many have an inability to take into account.

Moreover, a thin intermediate layer (Cr, Ti, or Ni typically) is used to stick gold on substrate. This adhesion layer shifts and broadens the LSPR peak [25, 27] as well as the Surface Plasmon Resonance of thin films [15,28,29]. The critical role of the adhesion layer is undeniable [26,30] even if some theoretical studies revealed that a chromium layer with thickness smaller than 10 nm only slightly influences the LSPR position for an array of nano-cylinders [27]. On the other hand, the adhesion layer plays a crucial role on the plasmonic fluorescence enhancement [30].

Therefore, both roughness and adhesion layer should not be neglected in a first approach. The need to describe the roughness numerical models restricts the choice of methods, even if some conventional methods were modified to describe this property of scattering objects: finite difference time domain (FDTD) [31], coupled wave method (CWM) [32], finite element method (FEM) [33, 34], boundary element method (BEM) [35] for which the meshing of the rough surface may be critical for computation. In [32] was claimed that a roughness of 1 nm produces negligible disturbance of the surface plasmon, but authors also underlined that the imperfection of the fabrication process may produce very rough surfaces and therefore could induce notable variations in the computed properties of localized plasmons between smooth and rough surfaces, and therefore with experiments. However the most famous (and the oldest) method used to describe light-matter interaction with nanoparticles with irregular shape and sometimes rough is probably the discrete dipole approximation (DDA) [18, 36–42].

DDA was firstly developed by Devoe [43, 44] and Purcell [45]. The main idea is to discretize the nanoparticle into a set of N elements or dipoles with polarizabilities α_j, located at $\mathbf{r}_j$. Each dipole has a polarization $\mathbf{P}_j = \alpha_j \mathbf{E}_j$, where $\mathbf{E}_j$ is the electric field at $\mathbf{r}_j$ induced by the incident wave and the sum of the dielectric fields induced by interaction with other dipoles. Consequently, a system of complex linear equations must be solved to find polarizations $\mathbf{P}_j$ and evaluate the extinction cross section following [36]:

$$C_{ext} = Q_{ext}\pi\frac{D^2}{4} = \frac{4\pi k_0}{|\mathbf{E}_0|^2}\sum_{j=1}^{N}\left\{\Im\left[\mathbf{P}_j.(\alpha_j^{-1})^*\mathbf{P}_j^*\right]\right\}, \quad (1)$$

with Q_{ext}, the extinction efficiency [22], $k_0 = 2\pi/\lambda_0$ the modulus of the wave vector and $\mathbf{E_0}$ the amplitude, of the illumination monochromatic plane wave. $\Im(.)$ is the imaginary part of a complex number. C_{ext} is written under the assumption of linearly polarized incident light [36]. The method was extended to periodic structures by Markel [46] and Chaumet [41, 47].

#179498 - $15.00 USD Received 7 Nov 2012; revised 21 Dec 2012; accepted 9 Jan 2013; published 23 Jan 2013

Investigation of the validity criterion of discrete dipole approximation method (DDA) confirmed than that method is suitable for highly irregular particles, when many other approaches are not available [48]. Comparison with experiments reveals a high sensitivity of results with dielectric functions of metal [49]. Nanoparticles with arbitrary shapes where modeled for extinction and Raman spectroscopy applications [50] and the influence of porosity of thin cylinders was recently investigated with DDA [51]. In a recent paper, the comparisons of numerical results with two series of experimental data reveal that modeling the roughness of samples gives better agreement [16] and propose therefore, an alternative to the approximative knowledge of permittivity, for the explanation of the decay between experiments and calculations [49]. Therefore, we propose to use the DDA for the following study.

The Fortran code DDSCAT 7.1, developed by Draine and Flatau, is used for calculating extinction of light by irregular particles based on the DDA [52]. DDSCAT offers the possibility of editing new shapes. Therefore, to handle with roughness, a uniform probability law is used to remove or to add a dipole from/to the surface, or to keep it unchanged (Fig. 2) [16]. Therefore, the root of mean square roughness is RMS=$\sqrt{\frac{(-2)^2+0+2^2}{3}} \approx 1.6$ nm, that is close to the RMS resulting from the lithography process that can be observed in MEB images of samples. The adhesion layer is also discretized as shown in Fig. 2.

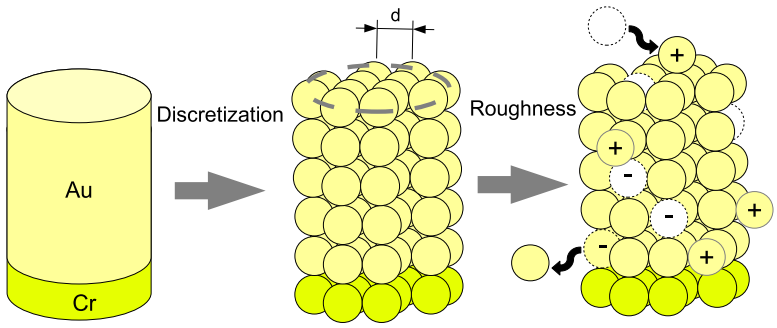

Fig. 2. Biosensor: grating of gold cylinders with diameter D, height h and period $P+D$. The gold nanostructures are deposited on a glass substrate. A layer of Chromium of thickness e is used to improve adhesion of gold on glass. The centers of the dipoles (discretization for DDA) are on regular mesh and the roughness is obtained by removing (yellow) or adding (red) a dipole on the surface. For computations the inter-dipole distance is $d = 2$ nm.

The inter-dipole distance $d = 2$ nm is smaller than 2.6 nm that ensured the validity of the calculations in [5]. The target precision for the inversion of the matrix of coupling between dipoles is 10^{-3}. The magnitude of the electric field at distance r from any dipole decreases as a polynomial function of $1/r$. The factor $\exp\left[-(\gamma k_0 r)^4\right]$ was introduced to vanish the coupling between remote dipoles in a periodic lattice (with $k_0 = 2\pi/\lambda_0$ the modulus of the illumination wave vector) and therefore to increase the speed and accuracy of computation [41]. γ can be therefore seen as a cutoff parameter which smoothly suppresses the influence of far dipoles in periodic structures. In the present case, $\gamma = 0.1$ is chosen to achieve both sufficient accuracy in the investigated size range of parameters, and a reasonable computational time (less than one hour). Indeed, the computation of spectrums in the range 550 nm to 850 nm of wavelength requires 31 evaluations of the model, if a precision of 10 nm is supposed to be sufficient for the computation of the LSPR spectral position.

The DDA is based on the discretization of materials, and therefore including the thick sub-

#179498 - $15.00 USD Received 7 Nov 2012; revised 21 Dec 2012; accepted 9 Jan 2013; published 23 Jan 2013

strate in the model would require computational time. Consequently, the surrounding medium is modeled by an effective medium with relative permittivity ε_{eff} [18, 53] equal to the mean of that of the glass substrate [8] and that of air (Eq. (2)). The relative permittivity of glass ($1.43^2 = 2.04$) is considered as constant on the whole investigated domain of wavelengths ($\lambda_0 \in [550, 850]$ nm).

$$\varepsilon_{eff} \approx (\varepsilon_{air} + \varepsilon_{Glass})/2 = 1.52 \tag{2}$$

This formulation is also known in optics as the Geometrical Effective Medium Approximation (GEMA) which was developed for absorbing multilayer structures [54] and used to retrieve unknown experimental data from Turbadar's measurements of reflectance of thin aluminum layers [55].

The effective medium approximation may induce a blue-shift of the LSPR [5] but the comparison with other theoretical results may help to validate the proposed model of effective medium. We first compare DDA results to computations from Finite Difference Time Domain (FDTD) method [27]. In that reference, no roughness was introduced, the surface of cylinders was smooth, $D = 100$ nm and $h = 50$ nm. The period of the grating was $D + P = 300$ nm with $P = 200$ nm (Fig. 1). The relative permittivities of metals were found in the same references [56, 57] and the nanostructures were deposited on a glass substrate. The location of the LSPR in the absence of Cr adhesion layer occurs at $\lambda_0 = 586$ nm with FDTD and $\lambda_0 = 590$ nm with DDA. Therefore in the investigated domain of parameters, the effective medium seems to be a usable approximation.

The relative permittivities of chromium and gold are the bulk ones [56, 57]. The gold and chromium relative permittivity from [56] and [57] are plotted in Figs. 3 and 4. For gold, the Johnson and Christy data are chosen for their smoother behavior within the investigated wavelengths domain. A cubic spline is used to get the appropriate discretization of the dispersion curves with wavelength step of 10 nm. The result takes advantage of the continuity of derivative compared to a linear fitting of the reference data.

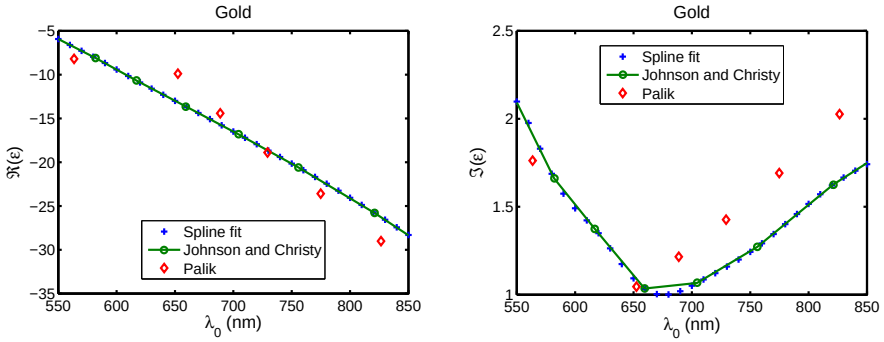

Fig. 3. Reference data for the relative permittivity of gold and cubic spline fitting of Johnson and Christy data [56]. The Palik's data are also shown [57]. The result of fit is used for the numerical computations.

#179498 - $15.00 USD Received 7 Nov 2012; revised 21 Dec 2012; accepted 9 Jan 2013; published 23 Jan 2013

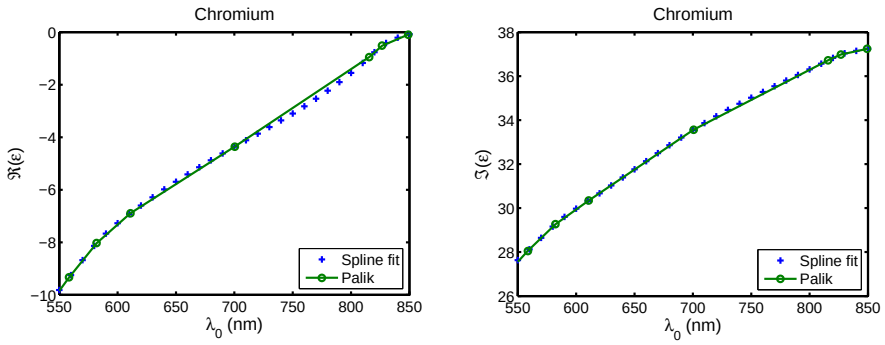

Fig. 4. Reference data for the relative permittivity of chromium and cubic spline fitting of Palik data [57]. The result of fit is used for the numerical computations.

Chromium is more absorbing than gold and therefore the extinction spectrum is broadened and attenuated for surface plasmon resonance (SPR) [15, 58–60] and localized surface plasmon resonance (LSPR) [25–27, 59]. These parameters are also subject to uncertainties and the position of the LSPR $\lambda_0(LSPR) = \lambda_0(\max(C_{ext}))$ could depend on them [39, 49] but their numerical values are unknown in our case.

Therefore the final validation of the results of the proposed method by comparison with series of experimental data remains the only alternative.

To perform a parametric study, the discretization of the parameter space (D, h, e λ_0) must be determined, by a first evaluation of the propagation of experimental uncertainties through the numerical model. The target is the position of the LSPR.

4. Discretization and key parameters

The experimental uncertainties mentioned above (section 2) can help to define the step size of D, h, e and λ_0 in order to maintain the computational time of the parametric study in a reasonable range and to obtain significant results. For this, we compute the propagation of experimental uncertainties through the model to check their influence on the shift of the LSPR. Two diameters are considered for this evaluation with the above described model: $D = 100$ nm and $D = 200$ nm, near the boundaries of the investigated domain of the parametric study. The height of cylinders is the reference in experiments $h = 50$ nm [8]. A step of 10 nm is used for the computations of the spectrum $C_{ext}(\lambda_0)$. The cylinders are supposed to have smooth surfaces. The corresponding uncertainty on the position of LSPR ($\lambda_0(LSPR)$) is therefore ± 5 nm in the numerical calculations. This approach corresponds to the evaluation of the partial derivative of the function $\lambda_0(LSPR)(D, h, e, RMS)$ around typical values in the hyperspace of parameters.

Table 1. Sensitivity of the position of the localized plasmon resonance (LSPR) when propagating uncertainties through the DDA model of rough biosensor with gold cylinder (diameter D, height h) on chromium adhesion layer of thickness e.

$D = 100$ nm, $h = 50$ nm, $P = 200$ *nm* [8]				
Parameter (nm)	$D \in [80;120]$	$h \in [48;52]$	$e \in [0;4]$	RMS $\in [0;1.6]$
Shift of $\lambda_0(LSPR)$	± 20 nm	± 30 nm	± 10 nm	± 20 nm
$D = 200$ nm, $h = 50$ nm, $P = 200$ *nm* [8]				
Parameter (nm)	$D \in [180;220]$	$h \in [48;52]$	$e \in [0;4]$	RMS $\in [0;1.6]$
Shift of $\lambda_0(LSPR)$	± 30 nm	± 10 nm	± 10 nm	± 10 nm

#179498 - $15.00 USD Received 7 Nov 2012; revised 21 Dec 2012; accepted 9 Jan 2013; published 23 Jan 2013

The results in Table 1 show that h and D are key parameter for $\lambda_0(LSPR)$ as well as the roughness. The influence of the nanometric layer of chromium is less critical for the position of LSPR [27] than on the damping of the resonance and therefore on the sensitivity of the biosensor [15]. The roughness cannot be neglected for the smallest diameter.

The combined uncertainty $u_B(\lambda_0(LSPR))$ on the LSPR shift can therefore be evaluated from the above uncertainties of type B [61], by considering *a priori* uniform law of probability within the above intervals and no correlation between these parameters. The following results are obtained:

- $D = 100$ nm, $h = 50$ nm, $P = 200$ *nm*:

$$u_B(\lambda_0(LSPR), D = 100nm) = \frac{1}{\sqrt{3}}\sqrt{20^2 + 30^2 + 10^2 + 20^2} \approx 24nm \tag{3}$$

- $D = 200$ nm, $h = 50$ nm, $P = 200$ *nm*:

$$u_B(\lambda_0(LSPR), D = 200nm) = \frac{1}{\sqrt{3}}\sqrt{30^2 + 10^2 + 10^2 + 10^2} = 20nm \tag{4}$$

In both cases, uncertainties may produce a shift greater than ± 20 nm within the investigated range of diameters. The combined uncertainty is stable, even if the sensitivity to each source of uncertainty differs. Consequently, the influence of the experimental uncertainties on the position of the LSPR can be observed considering a sampling step of 10 nm for λ_0. The corresponding uncertainty on the position of LSPR ($\lambda_0(LSPR)$) is therefore ± 5 nm in the numerical calculations. No further fitting of the extinction cross section $C_{ext}(\lambda_0)$ curve is used. The evaluation of the experimental uncertainty (Eqs. (3) - (4)) is used in the following for the plot of experimental data. The computation of the position of the LSPR requires 31 computations of the extinction cross-section C_{ext} for $\lambda_0 \in [550;850]$ nm. The rough sample is considered in the following.

The numerical experience plan consists in nested loops on D, h, e, λ_0. Table 2 gives the intervals and the discretization step for all parameters. The total number of computations is $N = 15500$.

Table 2. Domain of variation of the parameters and discretization step. D, h are the diameter and the height of cylinders, e is the thickness of the chromium adhesion layer and λ_0 is the wavelength in vacuum. The RMS is the root of mean square of the roughness. The number of computation in the nested loops is therefore $N = 15500$.

Param. (nm)	$D \in [50;250]$	$h \in [20;70]$	$e \in [0;8]$	RMS $\in [0;1.6]$	$\lambda_0 \in [550;850]$
Discret. step	20 nm	10 nm	2 nm	1.6 nm	10 nm
numb. of comp.	10	5	5	2	31

The N computations being realized on a computer with 30 processors, a database of results can be exploited. This approach is far from the optimization of the nanostructures which requires a specific optimization method for computational time sparing, to get the best parameters set [42, 62, 63]. The following establishment of an heuristic law governing the LSPR is based on the least square fitting of the database, using information on the critical parameters. The database obtained from the experience plan contains 500 simulations of the position of the LSPR for different gratings of nanocylinders.

#179498 - $15.00 USD Received 7 Nov 2012; revised 21 Dec 2012; accepted 9 Jan 2013; published 23 Jan 2013

5. Heuristic law for $\lambda_0(LSPR)$

Some papers were dedicated to a systematic study of the optical properties (absorption, extinction or scattering) of nanoparticles [25, 38–40, 49]. All these studies are direct parametric studies and reveal the dependance of the LSPR of nanoparticles on the various parameters of the problem. In that studies, the position of the LSPR as a function of the aspect ratio, diameter or length of the nanoparticles was observed but never exploited through an inverse problem procedure [64].

A first analysis of the 500 computed spectra confirms that, with or without roughness, a chromium adhesion layer e lower than 6 nm produces only a shift of the LSPR lower than 20 nm. A theoretical study [27] and our results show that including the adhesion layer blueshifts the LSPR for small diameters ($D = 100$ nm). Increasing the diameter D or decreasing the height h of cylinders redshift the LSPR [18, 25]. The same behavior was observed for smooth nanodisks with $D = 175$ nm, h ranged from 10 nm to 150 nm [25].

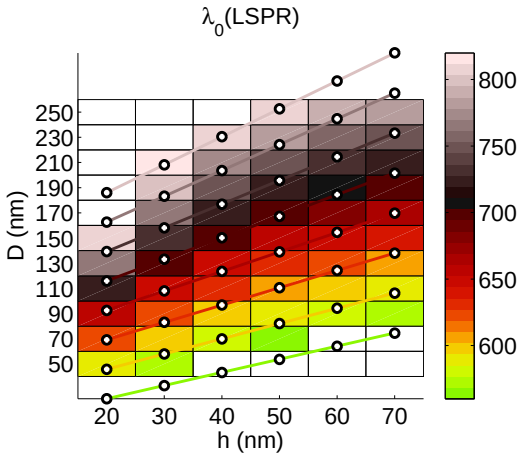

Fig. 5. Plots of the LSPR wavelength $\lambda_0(LSPR)$ in gray level as a function of cylinder diameter D and height h. The mean value of $\lambda_0(LSPR)$ is calculated for chromium thicknesses $e = 2$ nm and $e = 4$ nm to describe experiments in [8], where the thickness of chromium was evaluated to 3 nm, with uncertainty of more than 1 nm. The separation between cylinders is $P = 200$ nm. The lines are the results of fits deduced from Eq. (5).

Figure 5 shows a quasi-linear behavior of the relation between D and h for a given LSPR wavelength. The selection of the pairs of (D,h) corresponding to a given $\lambda_0(LSPR) = \lambda_0(\max(C_{ext}))$ are fitted with an affine function by minimizing the least square residue [65]. The method uses a robust fit of the results of the parametric study. The algorithm uses iteratively reweighted least squares with the bisquare weighting function (Matlab). The resulting class of slope and intercept can then be fitted with an affine function of the LSPR wavelength $\lambda_0(LSPR)$:

$$D = (a_1\lambda_0(LSPR) + b_1)h + (a_2\lambda_0(LSPR) + b_2) \quad (5)$$

The resulting heuristic law is deduced directly from the parametric study: a steady position of the LSPR is observed if the Eq. (5) between D (nm) and h (nm) is satisfied. This law is deduced from the least square fitting of the results of the parametric study, simply by computing the slope and the intercept of D as a function of h for each LSPR position, and then by finding

#179498 - $15.00 USD Received 7 Nov 2012; revised 21 Dec 2012; accepted 9 Jan 2013; published 23 Jan 2013

the linear dependence of a and b on the LSPR position $\lambda_0(LSPR)$. A similar approach was used to characterize the near-field optical microscopes and the evanescent near-field around nanostructures [13, 66].

The values of a_i and b_i and their dispersion are given in Table 3.

Table 3. Fitting of the numerical experience plan with function defined in Eq. (5). The relative standard uncertainty on each coefficient [61] is indicated for all coefficients assuming uniform law of probability, including the uncertainty on the position of the LSPR (step of 10 nm).

a_1 (nm)$^{-1}$	b_1 (unitless)	a_2 (unitless)	b_2 (nm)
0.0084	-3.9	0.32	-160
27%	36%	30%	35%

Equation (5) is the solution of the inverse problem as it enables to calculate the geometrical parameter D for a target wavelength of LSPR. If h should be calculated as a function of $\lambda_0(LSPR)$, Eq. (6):

$$h = \frac{D - b_2 - a_2\lambda_0(LSPR)}{b_1 + a_1\lambda_0(LSPR)} \tag{6}$$

Figure 5 shows the plots of Eq. (5), superimposed on the data of the experience plan. The linear behavior of D as a function of h is dependent on the LSPR position. Equation (5) helps to determine the geometrical parameters (D and h) of the biosensor to adjust the LSPR to a given wavelength. The domain of validity of this law is the hypercube defined in Table 2 considering rough structures. Equation (5) gives a function which reciprocal can be calculated for deducing the position of the LSPR as a function of D and h.

$$\lambda_0(LSPR) \quad = \quad \frac{D - b_2 - b_1 h}{a_2 + a_1 h} \tag{7}$$

A class of parameters can be therefore deduced from the formula (5), (6) and (7) and could help to design the biosensor. The formula (7) can also be used to calculate the propagation of experimental uncertainties for the LSPR position and therefore to evaluate the tolerance of fabrication of such device [67]. Before going further, a validation of the proposed affine approximations must be proposed by comparison with experimental data.

5.1. Validation by comparison with experimental data

A comparison of the heuristic law (Eq. (7)) and experimental data in [8] shows a good agreement (Fig. 6). The values of h for the red curve are slightly lower than the experimental expected value by considering free height h. This behavior is coherent with the fact that the shape of nanoparticles is not exactly a cylinder but rather a smooth island of gold, especially for small diameters and heights.

#179498 - $15.00 USD Received 7 Nov 2012; revised 21 Dec 2012; accepted 9 Jan 2013; published 23 Jan 2013

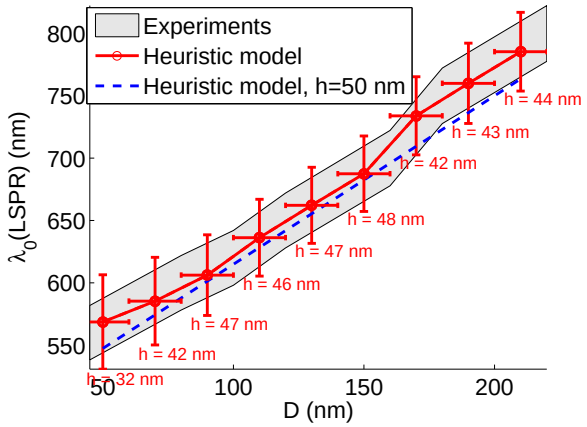

Fig. 6. Plots of the domain of experimental localized surface plasmon wavelength $\lambda_0(LSPR)$ in gray as a function of the cylinder diameter D [8]. The size of the gray zone is deduced from experimental uncertainties. Computed values of $\lambda_0(LSPR)$ are deduced from Eq. (7) for the height of cylinders $h = 50$ nm (blue line) and the red crosses show the uncertainties around values of $\lambda_0(LSPR)$ computed for the indicated value of h.

The comparison with experimental data obtained by varying the height of cylinders (from [4]), shows also a good agreement for $D = 100$ nm (Fig. 7). The red curve is obtained for the best fitting of the experimental data by considering free diameter D. The corresponding values of D are close to the experimental value of D according to its uncertainty.

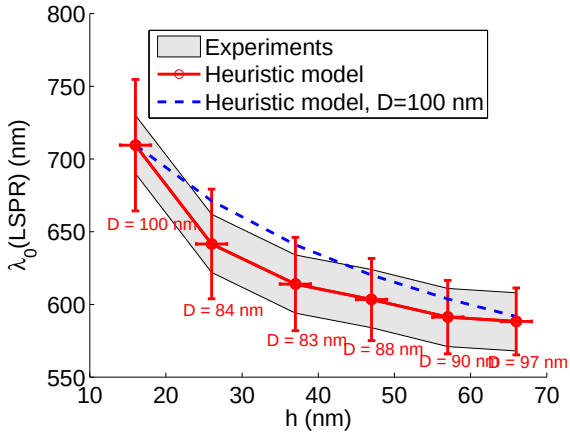

Fig. 7. Plots of the domain of experimental localized surface plasmon resonance wavelength $\lambda_0(LSPR)$ in gray as a function of the height of cylinders h [4]. The size of the gray zone is deduced from experimental uncertainties. Computed values of $\lambda_0(LSPR)$ are deduced from Eq. (7) for the cylinders diameter $D = 100$ nm (blue line) and the red crosses show the uncertainties around values of $\lambda_0(LSPR)$ computed for the indicated value of D.

The two comparisons with experimental data for various values of h and D can be considered as hard tests of validity. The agreement of numerical and experimental results is satisfying and is coherent with the properties of the process of deposition of gold on substrate. Moreover

#179498 - $15.00 USD Received 7 Nov 2012; revised 21 Dec 2012; accepted 9 Jan 2013; published 23 Jan 2013

the results show that the effective permittivity of the surrounding medium and the gold and chromium permittivities can be used to describe accurately the biosensor within the range of parameters.

In Ref. [8] the best Raman signal enhancement was obtained for the LSPR position exactly between the excitation wavelength λ_0 and the Raman wavelength λ_R related to the band of interest of the probe molecule observed. Félidj et al. proposed to adjust the LSPR at the mean value of both wavelengthes. For excitation at $\lambda_0 = 632.8$ nm and a Raman wavelength $\lambda_R = 685$ nm (BPE band at 1200 cm^{-1}), the best LSPR position was found to be located at 659 nm. For the first order, the corresponding nanocylinder diameter was found to be close to 130 nm. The heuristic law gives $D = 133 \pm 3$ nm for $h = 50$ nm and $u(h) = \pm 2$ nm. The second experience uses illumination at $\lambda_0 = 785$ nm. Therefore $\lambda_R = 867$ nm and the LSPR is tuned to 826 nm. Formula (5) gives $D = 256 \pm 6$ nm, which is closer to the measured value of the best SERS gain obtained for $D = 220$ nm than the announced target (300 nm) in [8]. The predictive ability of the heuristic law which describes the relationship between the LSPR position $\lambda_0(LSPR)$, D and h seems to be valid in the whole domain of parameters given in Table 1. To illustrate the possible use of this law, we investigate some specific geometries before evaluating the propagation of uncertainties.

5.2. Case of homothetic cylinders

Equation (7) seems to be a good approximation of the variation of the LSPR as a function of the geometrical parameters D and h, for a grating of rough gold cylinders with adhesion layer ($e = 2$ nm) and $P = 200$ nm (Fig. 1). The specific case of homothetic cylinders with $h = D$, removes a degree of freedom and leads to a simpler formula, with a_1, a_2, b_1, b_2 given in Table 3:

$$\lambda_0(LSPR, h = D) \quad = \quad \frac{(1 - b_1)D - b_2}{a_2 + a_1 D} \tag{8}$$

This formula is strictly valid in the interval $h = D$ ranging from 50 to 70 nm, by cons it should still be checked for larger heights.

5.3. Case of nanodisks

Asymptotic form of $\lambda_0(LSPR)$ could be of interest especially for specific aspect ratio of the cylinder. For example, for nanodiscs ($h << D$), the position of the LSPR can be deduced from the series of Eq. (7).

$$\lambda_0(LSPR, h << D) = \frac{D - b_2}{a_2} - \frac{(a_2 b_1 + a_1(D - b_2))}{a_2^2} h + o[(h/D)^2], \tag{9}$$

where $o[(h/D)^2]$ represents omitted terms of order higher than 2 in the series and a_1, a_2, b_1, b_2 are given in Table 3.

This equation confirms that the correction induced by the height assuming a small aspect ratio h/D is a blueshift of the LSPR, whatever are the diameters D. These formula can be used to select the best parameters for a given LSPR position. Figure 8 shows the plots of the position of the LSPR as a function of the aspect ratio D/h of the cylinder. The linear behavior can be compared to that observed for nanorods [68] for a wider range of aspect-ratio. This confirms the good behavior of the model in the range of parameters.

#179498 - $15.00 USD Received 7 Nov 2012; revised 21 Dec 2012; accepted 9 Jan 2013; published 23 Jan 2013

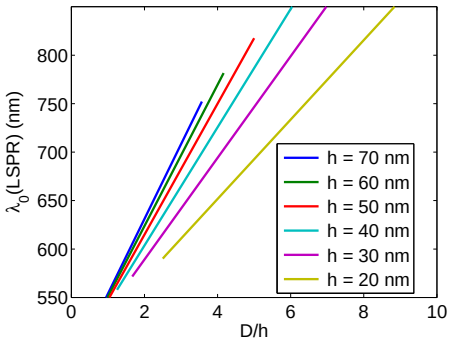

Fig. 8. Position of the LSPR computed from the heuristic law (Eq. (11)) as a function of the aspect ratio D/h of the cylinder for various heights h. The parameters of the model are $P = 200$ nm with roughness ($rms = 1.6$ nm) and chromium adhesion layer ($e = 2-4$ nm).

Another interest of these simple laws is the fact that propagation of uncertainties of the fabrication process can be evaluated directly, and therefore, the sensitivity analysis of LSPR position on the geometrical parameters h and D can be deduced, at least within the investigated domain of geometrical parameters and wavelengths. This is investigated in what follows.

5.4. Sensitivity of LSPR to uncertainties on size parameters

The propagation of uncertainties and the sensitivity analysis of a process or a physical phenomenon helps to improve the fabrication process of any device, by exhibiting the parameters that should be controlled first. Indeed the identification of critical parameters which uncertainty should be reduced is relevant, for a challenging improvement of technology.

First, the propagation of experimental uncertainties of fabrication can be deduced from the partial derivatives of $\lambda_0(LSPR)(D,h)$ (Eq. (7)). The uncertainty on $\lambda_0(LSPR)$ is deduced form the experimental uncertainties on D ($u(D)$) and h ($u(h)$) [61, 5.1.2]:

$$u(\lambda_0(LSPR)) = \sqrt{\left(\frac{\partial\lambda_0(LSPR)}{\partial D}\right)^2 u^2(D) + \left(\frac{\partial\lambda_0(LSPR)}{\partial h}\right)^2 u^2(h)} \tag{10}$$

$$= \sqrt{\left(\underbrace{\frac{1}{a_2+a_1h}}_{S_D}\right)^2 u^2(D) + \left(\underbrace{\frac{a_1b_2-a_2b_1-a_1D}{(a_2+a_1h)^2}}_{S_h}\right)^2 u^2(h)} \tag{11}$$

where the partial derivatives are called sensitivity coefficients and a_1, a_2, b_1, b_2 are given in Table 3 Knowing the experimental uncertainties on h and D, the uncertainty on the LSPR can be deduced. The sensitivity coefficients S_h and S_D can be used to evaluate the effect of the experimental dispersion of values of D and h around a mean value. They contribute to the improvement of the uncertainty evaluation of the LSPR position given in Eqs. (3) - (4). For $D = 100$ nm and $D = 200$ nm, $u(\lambda_0(LSPR)) \approx 27$ nm and 28 nm respectively. The study of the properties of S_D and S_h gives insight on the sensitivity of the uncertainty $u(\lambda_0(LSPR))$ to uncertainties on D and h. The balance between the two terms of the sum in Eq. (11) could give information on the critical process that needs to be improved in priority.

#179498 - $15.00 USD Received 7 Nov 2012; revised 21 Dec 2012; accepted 9 Jan 2013; published 23 Jan 2013

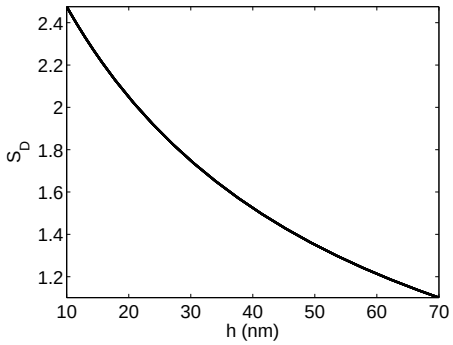

Fig. 9. Sensitivity coefficient S_D of uncertainty on the position of the LSPR computed from the heuristic law (Eq. (11)) as a function of the cylinders height h.

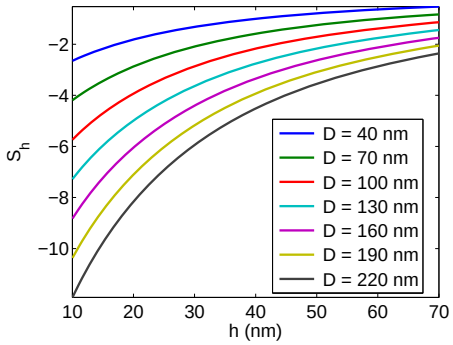

Fig. 10. Sensitivity coefficient S_h of uncertainty on the position of the LSPR computed from the heuristic law (Eq. (11)) as a function of cylinders height h, for various diameters D.

The plot of S_D (Fig. 9) show a slow decreasing of the sensitivity with h. The mean sensitivity of $u(\lambda_0(LSPR))$ on D is therefore about 1.45 in the considered range of parameters. The same behavior is exhibited in Fig. 10, $|S_h|$ decreases with h. The mean value of the sensitivity is around -4 and decreases with D. In terms of uncertainties, the weight of each term in the sum in Eq. (11) is of the same order of magnitude. Therefore, the uncertainty on the shape of cylinders (and on the diameter) should be decreased in priority in order to get a better control of the biosensor efficiency. This improvement is critical for cylinders with smaller height.

The present control on the thickness of gold deposition is about ± 2 nm and that of diameters is about ± 20 nm. In this case, the uncertainty on the LSPR position remains lower than 35 nm for all diameters if $h \in [10;70]$ nm (Fig. 11). The relative uncertainty is about two times greater for small diameters and the absolute uncertainty decreases slightly as h increases.

#179498 - $15.00 USD Received 7 Nov 2012; revised 21 Dec 2012; accepted 9 Jan 2013; published 23 Jan 2013

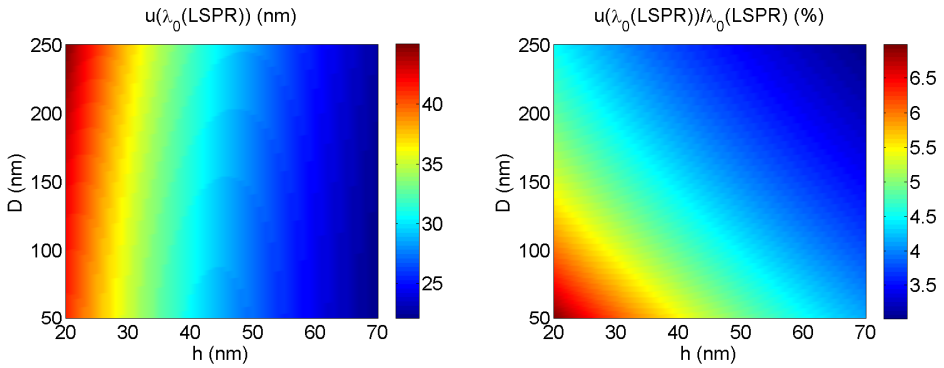

Fig. 11. Uncertainty and relative uncertainty on the position of the LSPR computed from the heuristic law (Eq. (11)). The parameters of the model are the cylinders separation $P =$ 200 nm and the chromium adhesion layer thickness ($e \in [2;4]$ nm). The roughness is $RMS =$ 1.6 nm.

Figure 11 show that the tolerance on the small geometrical parameters (D,h) does hardly differ from that on bigger ones. Therefore, the whole process of fabrication, whatever is the LSPR position, will take advantage of the improvement of the lateral control of metal deposition.

In this section, we have obtained an heuristic law to describe the link between the position of the LSPR and the size parameters D and h of the cylinders. This law seems to be valid even if an adhesion layer of chromium of thickness $e = 2-6$ nm is used. Moreover, the simplicity of this law helps to determine a first approximation of the size of the cylinder for tuning the LSPR position, as well as the effect of the propagation of experimental uncertainties on the position of the LSPR.

6. Conclusion

The Discrete Dipole Approximation (DDA) is used for a parametric study of the biosensors made of a grating of nanocylinders. The Localized Surface Plasmon Resonance (LSPR) measurement is modeled by the maximum of the extinction cross-section over the considered spectrum. Considering a fixed distance between cylinders, the investigated parameters are the height h, the diameter D, the thickness e of the chromium adhesion layer, and the roughness of the nanocylinders. Thin adhesion layers slightly modify the position of the LSPR. Roughness induces a redshift which enables to fit experimental results despite the use of bulk permittivities for chromium and gold and an effective index model for the system substrate-air. The relative influence of h and D is more complex but can be deduced from an heuristic law for the LSPR position. This law is obtained through an affine fitting of the proposed numerical experience plan. The agreement with experimental results [4, 8] is satisfactory, falling within the experimental uncertainties of fabrication. Therefore the heuristic law of behavior of the LSPR position can be used with confidence. Then the reciprocal function of the position of the LSPR can be used to a first computation of class of diameters and heights of cylinders to design sensors. This approach could be extended to more complex shape of nanoparticles, at the expense of computation time and complexity of interpretation. The propagation of uncertainties of fabrication being determined for the investigated parameters, the influence of the functionalization layer that is used to fix the bio-molecules of interest in the vicinity of metallic nanoparticles will be the object of further studies. Higher order fits should also be investigated, at the possible expense of the uniqueness and simplicity of the solution of the inverse problem.

#179498 - $15.00 USD Received 7 Nov 2012; revised 21 Dec 2012; accepted 9 Jan 2013; published 23 Jan 2013

Acknowledgments

This study is partially supported by the Conseil Régional de Champagne-Ardennes, the Conseil Général de l'Aube, and the *Nanoantenna* European Project (FP7 Health-F5-2009-241818).

#179498 - $15.00 USD Received 7 Nov 2012; revised 21 Dec 2012; accepted 9 Jan 2013; published 23 Jan 2013